

Experimental confirmation of electron figure-8 motion in a strong laser field

Brittini Pratt, Nicholas Atkinson, Daniel Hodge, Mahonri Romero , Christoph Schulzke ,
Yance Sun, Michael Ware *, and Justin Peatross [†]

Department of Physics and Astronomy, Brigham Young University, Provo, Utah 84602, USA

 (Received 31 October 2020; accepted 10 March 2021; published 29 March 2021)

We measure polarization-resolved fundamental, second, and third harmonic nonlinear Thomson scattering out the side of a laser focus with 10^{18} W/cm². The separate measured polarization components are each associated with a distinct dimension of predicted electron figure-8 motion. Taken together, the measured angular emission patterns for the two polarizations unambiguously confirm the figure-8 motion. Electrons are donated from low-density helium (10^{-3} to 1 Torr) ionized early during the laser pulse. Time-resolved single-photon detection is used to distinguish signal from noise.

DOI: [10.1103/PhysRevA.103.L031102](https://doi.org/10.1103/PhysRevA.103.L031102)

A half century has passed since the landmark publication by Sarachik and Shappert describing the theory of nonlinear Thomson scattering by electrons in a strong laser field [1]. They built on work from prior decades showing that, at relativistic intensities, electrons execute a figure-8 motion [2] while scattering both odd and even harmonics [3]. Electrons drift forward [4] as they oscillate in the laser field, responding to both the electric and magnetic components of the Lorentz force.

Through the years, there have been many theoretical studies of this fundamental interaction, which speaks to its intrinsic importance [5–19]. Experimentally, a number of teams have investigated nonlinear Thomson scattering from energetic electron beams colliding with intense laser pulses, where the scattering is highly directional and extremely blue shifted [20–27]. Relatively few experimental observations of nonlinear Thomson scattering have taken place in a frame of reference that does not strongly differ from the electron average rest frame [28–32]. Only one of these studies, Chen *et al.* in 1998 [29], measured the spatial structure of nonlinear Thomson emission. They observed second and third harmonic light scattered out the side of a laser focus at various angles. We extend their work by making the first polarization-resolved measurements of nonlinear Thomson scattering, for the fundamental, second-harmonic, and third-harmonic scattered photons.

To provide context for resolving nonlinear Thomson scattering by polarization, we summarize the equations of motion for a charged particle in a driving electromagnetic field:

$$\frac{d\mathbf{p}}{dt} = q(\mathbf{E} + \mathbf{u} \times \mathbf{B}), \quad (1)$$

where

$$\mathbf{p} = m\gamma\mathbf{u} \quad \text{and} \quad \gamma = \frac{1}{\sqrt{1 - u^2/c^2}}. \quad (2)$$

m denotes particle mass, q its charge, and \mathbf{u} its velocity. We neglect radiation reaction.

We first consider an electron subjected to a linearly polarized unfocused plane-wave pulse traveling in the z direction. The electric and magnetic fields may be expressed as

$$\mathbf{E} = \hat{\mathbf{x}}E_{\text{env}}(\varphi) \cos \varphi \quad \text{and} \quad \mathbf{B} = \hat{\mathbf{y}}\frac{E_{\text{env}}(\varphi)}{c} \cos \varphi, \quad (3)$$

where the field phase is given by

$$\varphi = \frac{\omega}{c}z - \omega t. \quad (4)$$

The quantity $\alpha(\varphi) \equiv \frac{qE_{\text{env}}(\varphi)}{m\omega c}$ is useful for representing the strength of the field, with relativistic effects becoming important when $\alpha \cong 1$ and above. The slowly varying envelope approximation permits writing $\int_{\varphi_0}^{\varphi} \alpha(\varphi') \cos \varphi' d\varphi' \cong \alpha(\varphi) \sin \varphi$ when solving for the electron trajectory, where it is assumed that $\alpha(\varphi_0) = 0$ before the interaction.

Sarachik and Shappert [1] showed that an electron initially at rest acquires a drift velocity during the pulse in the direction of field propagation given by

$$\mathbf{u}_{\text{drift}} = \hat{\mathbf{z}}\frac{c\alpha^2/4}{1 + \alpha^2/4}. \quad (5)$$

For convenience, they analyzed particle motion in the electron average rest frame, which moves at $\mathbf{u}_{\text{drift}}$ (equal to $\hat{\mathbf{z}}c/5$ when $\alpha = 1$). In this electron-drift frame, the particle trajectory is described by

$$\frac{\gamma\mathbf{u}}{c} = -\hat{\mathbf{x}}\alpha \sin \varphi - \hat{\mathbf{z}}\frac{\alpha^2}{4\sqrt{1 + \frac{\alpha^2}{2}}} \cos 2\varphi \quad (6)$$

and

$$\mathbf{r} = \frac{c}{\omega} \frac{\alpha}{\sqrt{1 + \frac{\alpha^2}{2}}} \left[-\hat{\mathbf{x}} \cos \varphi + \hat{\mathbf{z}} \frac{\alpha}{8\sqrt{1 + \frac{\alpha^2}{2}}} \sin 2\varphi \right]. \quad (7)$$

The laser frequency is redshifted in this frame, whereas α is invariant. Equations (6) and (7) describe the figure-8 trajectory

*ware@byu.edu

†peat@byu.edu

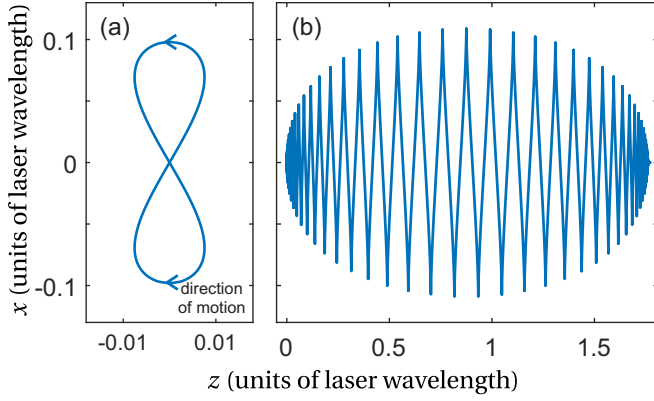


FIG. 1. (a) Electron trajectory computed in the average center-of-mass frame of a uniform plane wave (1×10^{18} W/cm 2 , $\alpha = 0.7$, 800 nm). (b) Electron trajectory computed in the laboratory frame for a plane-wave pulse ($\tau = 32$ fs).

for the electron, which is shown in Fig. 1(a) and which gives rise to scattered radiation.

In the electron center-of-mass frame the motion is periodic and the scattered light is comprised of discrete harmonics of order $n = 1, 2, 3, \dots$, to the extent that the driving-laser amplitude remains constant over many periods. The number of n th-harmonic photons scattered into the far field (per steradian per laser cycle) is given by [1,7,11,16]

$$\mathcal{N}_n = \frac{q^2 n}{8\pi^2 \epsilon_0 c h (1 + \frac{\alpha^2}{2})} \times \left| \int_0^{2\pi} \hat{\mathbf{R}} \times \left(\hat{\mathbf{R}} \times \frac{\gamma \mathbf{u}}{c} \right) e^{-in\varphi + in\frac{\omega}{c}(z - \mathbf{r} \cdot \hat{\mathbf{R}})} d\varphi \right|^2. \quad (8)$$

The unit vector $\hat{\mathbf{R}}$ specifies the direction to a detector. Sarachik and Shappert showed how to trade the integration in Eq. (8) for a series of Bessel functions. Alternatively, one may simply evaluate Eq. (8) numerically.

In spherical coordinates, we may write $\hat{\mathbf{R}} \times (\hat{\mathbf{R}} \times \mathbf{u}) = \hat{\theta}(-u_x \cos \theta \cos \phi + u_z \sin \theta) + \hat{\phi} u_x \sin \phi$ and $\mathbf{r} \cdot \hat{\mathbf{R}} = x \sin \theta \cos \phi + z \cos \theta$ [7]. In this work, we measure separately the longitudinal and azimuthal polarization components of the scattered photons. When a polarizer is placed in front of the detector and aligned either along $\hat{\theta} = \hat{x} \cos \theta \cos \phi + \hat{y} \cos \theta \sin \phi - \hat{z} \sin \theta$ or along $\hat{\phi} = -\hat{x} \sin \phi + \hat{y} \cos \phi$, one simply discards the orthogonal component.

The above formalism pertains to an unfocused plane-wave pulse. In our experiments, we have a tightly focused laser beam from which electrons can be expelled during the pulse, owing to strong ponderomotive gradients. Moreover, photons are observed in the laboratory frame rather than in a frame that moves in the direction of electron drift, whereas the speed of the drift varies with the time envelope of the short pulse and the electron location within the focus. However, since our experimental conditions are mildly relativistic, these effects only modestly influence the emission pattern, as will be demonstrated. Equation (8) compares well with our experimental data, although we simulate the experiment more robustly below.

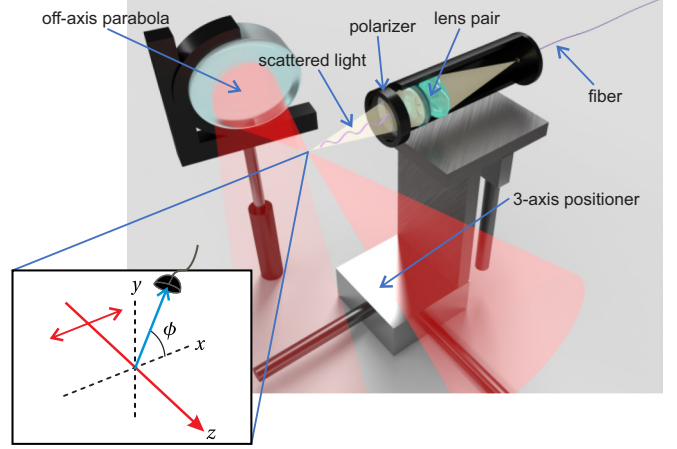


FIG. 2. Experimental setup inside vacuum. An off-axis parabola focuses the laser pulses. A half wave plate (not shown) rotates the linear polarization of the beam before focusing. Scattered photons traverse a wire-grid polarizer and are imaged onto the end of an optical fiber. The inset depicts an alternate viewpoint where instead the laser polarization remains fixed along the x axis while the detector rotates.

For our simulations, we represent the vector field for our focused laser by [33,34]

$$\mathbf{E} = \text{Re} \left\{ E_0 e^{-i\frac{\tilde{\omega}}{\omega\tau}} \left(\hat{\mathbf{x}} + \frac{xy}{2\mathbb{Z}^2} \hat{\mathbf{y}} - i \frac{x}{\mathbb{Z}} \hat{\mathbf{z}} \right) \frac{z_0}{\mathbb{Z}} e^{-\frac{kz_0 \rho^2}{2|\mathbb{Z}|^2}} e^{i\tilde{\varphi}} \right\}, \quad (9)$$

where $\mathbb{Z} = z_0 + iz$ and $\tilde{\varphi} = kz[1 + \rho^2/(2|\mathbb{Z}|^2)] - \omega t$. z_0 is the Rayleigh range, ρ the axial radius, and τ the pulse duration. The associated magnetic field is $c\mathbf{B} = \hat{\mathbf{x}}E_y + \hat{\mathbf{y}}E_x + \hat{\mathbf{z}}\frac{y}{x}E_z$. Trajectories for the classical electrons are computed using Eqs. (1) and (2), subject to Eq. (9). The far-field radiation pattern is dictated by [35]

$$\mathbf{E}_{\text{rad}} = \frac{q}{4\pi \epsilon_0 c^2 R} \frac{\hat{\mathbf{R}} \times [(\hat{\mathbf{R}} - \mathbf{u}/c) \times \mathbf{a}]}{(1 - \hat{\mathbf{R}} \cdot \mathbf{u}/c)^3}. \quad (10)$$

The right-hand side of Eq. (10) is evaluated at (retarded) time t , whereas the left-hand is a function of detector time $t' = t + \frac{R}{c} - \hat{\mathbf{R}} \cdot \frac{\mathbf{r}}{c}$, where $\frac{R}{c}$ can be ignored as an unimportant offset. The total energy per steradian (angular fluence) is $\Phi_\theta + \Phi_\phi$ where $\Phi_\theta = \epsilon_0 c R^2 \int_{-\infty}^{\infty} |\hat{\theta} \cdot \mathbf{E}_{\text{rad}}|^2 dt'$ and $\Phi_\phi = \epsilon_0 c R^2 \int_{-\infty}^{\infty} |\hat{\phi} \cdot \mathbf{E}_{\text{rad}}|^2 dt'$. The Fourier transform of \mathbf{E}_{rad} may be taken and a desired spectral window applied to restrict to a specific harmonic.

For our experimental conditions, electrons drift in the forward direction of the laser pulse according to Eq. (6) with α approaching 1. Figure 1(b) shows the trajectory of an electron at the focal center in the laboratory frame calculated using Eqs. (1) and (9). The electron oscillates in the x -dimension while drifting in the forward direction, owing to the force of the magnetic field. If the initial position of the electron is off center, strong gradients in the laser field cause electrons to flee out the side of the focus during the laser pulse.

Our experimental setup is shown in Fig. 2. An off-axis parabola (13° incident angle) focuses 800 nm Ti:sapphire laser pulses to a measured spot size of $w_0 = 3.2 \mu\text{m}$. The on-target pulse energy is approximately 15 mJ with duration

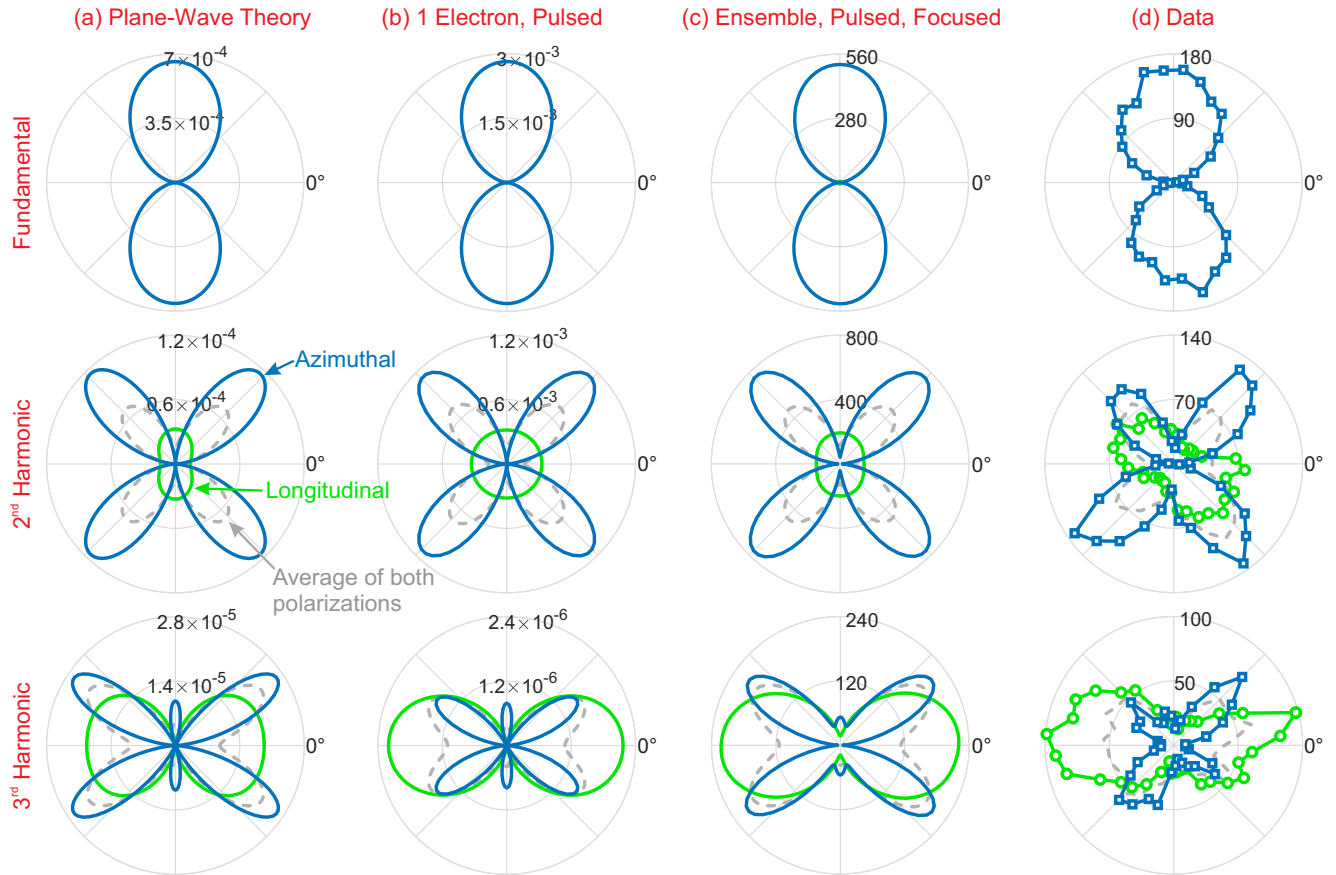


FIG. 3. Far-field angular emission patterns for first, second, and third harmonics in the plane perpendicular laser propagation (i.e., $\theta = 90^\circ$), resolved by polarization along $\hat{\phi}$ (blue, dark gray) and $\hat{\theta}$ (green, light gray). Column (a) shows the number of (redshifted) photons per steradian emitted during a single laser cycle of a plane wave ($I = 1 \times 10^{18} \text{ W/cm}^2$) according to Eq. (8). Column (b) shows the number of photons per steradian emitted during an entire laser pulse ($I_{\text{peak}} = 1 \times 10^{18} \text{ W/cm}^2$, $\tau = 32 \text{ fs}$) from an electron initially at the focal center ($w_0 = 3.2 \mu\text{m}$), computed according to Eq. (10). Column (c) gives the predicted number of photons emitted during 1000 laser shots from an ensemble of electrons distributed randomly throughout the laser focus ($\rho < 4w_0$ and $|z| < z_0$), with experimentally relevant electron density, collection/detection efficiency and spectral windowing applied to harmonics (see text). Column (d) shows the number of photons measured at various angles for 1000 laser shots.

$\tau = 32 \text{ fs}$ (FWHM = 38 fs) and peak intensity at the center of the focus of about $1 \times 10^{18} \text{ W/cm}^2$, with a factor of two uncertainty. Electrons are donated from low-pressure (10^{-3} to 1 Torr) helium to minimize possible plasma effects. We assume that helium's two electrons are liberated when the local intensity reaches about $1.3 \times 10^{15} \text{ W/cm}^2$ and $8.7 \times 10^{15} \text{ W/cm}^2$ [36]. A half wave plate rotates the laser polarization, and the polarization remains close to linear after reflection from the parabola, extinguishable with a linear polarizer to $< 0.4\%$.

Our experimental approach [37] uniquely combines techniques of quantum optics with high-intensity laser interactions. Measurements of the scattered radiation are made via photon counting, with the laser firing at 10 Hz. A section of the laser beam at the focus is imaged from the side using a 1:1 f/2.3 lens pair onto the end of a $105 \mu\text{m}$ glass fiber that leads to the detector. A wire-grid polarizer placed in front of the collection lens controls the polarization of the collected light. The fundamental and second harmonic photons were measured using an avalanche photodiode. The third harmonic was measured using a photomultiplier tube operating in Geiger mode.

Figure 3 shows calculated and measured radiation patterns in the plane perpendicular to the direction of laser propagation (i.e., with $\theta = 90^\circ$). For these polar plots, the laser is polarized at $\phi = 0^\circ$ (180°). Column (a) shows the number of photons per steradian *per laser cycle* emitted for the first, second, and third harmonic, according to Eq. (8). This corresponds to a single laser cycle in the electron average-center-of-mass frame near the peak of the laser pulse. Distinct emission patterns are seen for each polarization, along the $\hat{\phi}$ (azimuthal) and $\hat{\theta}$ (polar) directions. For comparison, the gray lines corresponds to unpolarized detection, calculated for an electron at the center of the focus using Eqs. (9) and (10), *for the entire pulse*.

To account for $\mathbf{u}_{\text{drift}}$ in the laboratory frame, we applied bandpass filters that are redshifted by about 12%. Spectral windows for the calculations matched the experimental setup: The fundamental was measured using a 40-nm-wide bandpass filter centered at 900 nm; the second harmonic was measured using a 40-nm bandpass filter centered at 450 nm; and the third harmonic was measured using a 10-nm bandpass filter centered at 310 nm (which avoided strong spectral noise from

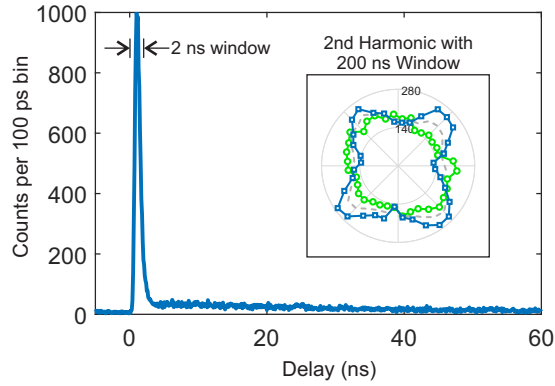


FIG. 4. Cumulative histogram showing arrival times for all photons measured for the second-harmonic data set plotted in Fig. 3. The inset repeats Fig. 3 column (d) for second-harmonic using a 200 ns time window.

helium near 300 nm). The nominal fundamental and harmonic wavelengths are 800, 400, and 266 nm.

In the experiment, electrons are initially distributed throughout the laser focus. Depending on position, electrons experience various peak intensities and are propelled from the focus at different velocities during the laser pulse, resulting in extremely distorted individual electron emission patterns [16]. However, when the emission is averaged from many trajectories, a symmetric emission pattern emerges, remarkably similar to the single-electron pattern in a plane wave. Column (c) in Fig. 3 shows the predicted number of photons (from 1000 laser shots) emitted from a large ensemble of electrons randomly distributed throughout the focal volume, according to the density of helium used for each measurement. The net emission from the many electrons is summed incoherently. Folded into the calculations are a 0.15-steradian collection lens and combined measured factors for fiber coupling efficiency C , filter transmission T , and detector quantum efficiency η that result in $CT\eta = 0.75\%$, 2.1% , and 0.44% for first, second, and third harmonics, respectively.

Column (c) of Fig. 3 can be compared directly with our measurements shown in column (d), which shows the number of photons registered from 1000 laser shots at various angles. Photons arriving promptly within a 2 ns window are counted while a comparatively large number of “noise” photons (from atomic deexcitation and recombination) arriving later are ignored. The backfilled pressure of the helium was adjusted so that about 10% of laser shots registered a photon in the prompt time window. The helium pressures used in the experiment were 1.08×10^{-2} Torr, 3.1×10^{-2} Torr, and 1.45 Torr for the first, second, and third harmonic, respectively.

The somewhat higher prediction of photon counts by our model than was measured might be attributable to uncertainties in collection efficiencies and laser intensity; we avoided free parameters in the comparison. The distortions in the measured patterns of Fig. 3(d), when compared to the simulations of Fig. 3(c), may indicate artifacts in our tight laser focus not easily seen through conventional direct imaging techniques. The distortion is greater for the third harmonic, likely related to its higher nonlinearity. The extent to which the laser vector fields in a focus may be characterized through such measurements is an intriguing question.

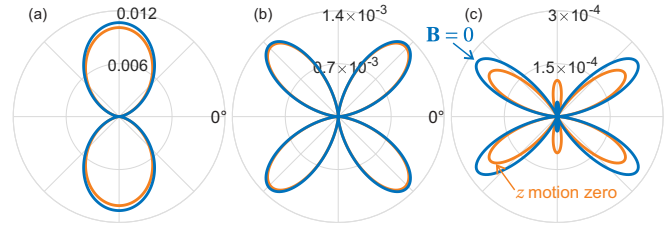


FIG. 5. Far-field emission pattern ($\hat{\phi}$ polarized) computed without the \mathbf{B} -field (blue, dark gray) and with the z component of the electron trajectory artificially set to zero (orange, light gray). Compare with column (b) of Fig. 3. The $\hat{\theta}$ polarization component vanishes.

Figure 4 shows a histogram of photon arrival times accumulated for all second-harmonic data points shown in Fig. 3. Note the noise tail that follows the prompt signal peak, presumably due to recombination emission. The inset demonstrates the importance of a narrow time window. We may infer that noise from prompt collisional electron-ion bremsstrahlung is minimal in our measurement, as evidenced by the near-zero emission at certain angles and polarizations in the data plots of Fig. 3.

The very different angular patterns for the two polarizations seen in Fig. 3 are associated with different dimensions of the figure-8 motion executed by the relativistic free electrons. In the plane perpendicular to the laser focus, the $\hat{\phi}$ component of the scattered light is exclusively associated with the \hat{x} component of Eqs. (6) and (7), while the $\hat{\theta}$ component is exclusively associated with the \hat{z} component. Figure 5 shows angular emission patterns computed using Eqs. (9) and (10) when the z -component of the electron motion is artificially removed in two different ways: (1) by setting the \mathbf{B} -field to zero while computing the trajectory, and (2) by setting the z -component of the electron trajectory to zero after computing the trajectory as usual. Both approaches yield qualitatively similar results. Namely, the $\hat{\theta}$ component of the trajectory vanishes while the $\hat{\phi}$ component remains about the same. Interestingly, the second harmonic along the $\hat{\phi}$ polarization persists, even when the terms $\cos 2\varphi$ and $\sin 2\varphi$ are eliminated from Eqs. (6) and (7). Under this same scenario, where electron motion is constrained to one-dimension, we find significant third-harmonic emission (and the lack of second-harmonic emission) on-axis, in the direction counter-propagating to the laser, as observed in Ref. [26].

In conclusion, we have experimentally confirmed the figure-8 motion of electrons in a high-intensity laser field. We have also shown that previous “confirmations” of the figure-8 motion [26,29] are based on observations that do not distinguish between one dimensional electron motion and actual two-dimensional figure-8 motion. We arrived at our conclusions based on an analysis of polarization-resolved nonlinear Thomson scattering, both experimentally and computationally. Polarization allows one to distinguish emission arising from electron motion associated with the laser \mathbf{E} -field versus motion associated with the laser \mathbf{B} -field.

This work is supported by the National Science Foundation under Grant No. 1708185.

- [1] E. S. Sarachik and G. T. Schappert, Classical theory of the scattering of intense laser radiation by free electrons, *Phys. Rev. D* **1**, 2738 (1970).
- [2] L. D. Landau and E. M. Lifshitz, *The Classical Theory of Fields*, 1st ed. (Addison-Wesley Press, Cambridge, 1951), pp. 120–121.
- [3] Vachaspati, Harmonics in the scattering of light by free electrons, *Phys. Rev.* **128**, 664 (1962).
- [4] J. H. Eberly and A. Sleeper, Trajectory and mass shift of a classical electron in a radiation pulse, *Phys. Rev.* **176**, 1570 (1968).
- [5] A. K. Puntajer and C. Leubner, Classical versus semiclassical predictions for harmonic generation in laser-free electron scattering under experimentally realizable conditions, *J. Appl. Phys.* **67**, 1606 (1990).
- [6] U. Mohideen, H. W. K. Tom, R. R. Freeman, J. Bokor, and P. H. Bucksbaum, Interaction of free electrons with an intense focused laser pulse in Gaussian and conical axicon geometries, *J. Opt. Soc. Am. B* **9**, 2190 (1992).
- [7] E. Esarey, S. K. Ride, and P. Sprangle, Nonlinear Thomson scattering of intense laser pulses from beams and plasmas, *Phys. Rev. E* **48**, 3003 (1993).
- [8] C. I. Castillo-Herrera and T. W. Johnston, Incoherent harmonic emission from strong electromagnetic waves in plasmas, *IEEE Trans. on Plasma Sci.* **21**, 125 (1993).
- [9] S. K. Ride, E. Esarey, and M. Baine, Thomson scattering of intense lasers from electron beams at arbitrary interaction angles, *Phys. Rev. E* **52**, 5425 (1995).
- [10] F. V. Hartemann, S. N. Fochs, G. P. Le Sage, N. C. Luhmann, Jr., J. Woodworth, M. D. Perry, and Y. J. Chen, and A. K. Kerman, Nonlinear ponderomotive scattering of relativistic electrons by an intense laser field at focus, *Phys. Rev. E* **51**, 4833 (1995).
- [11] Y. I. Salamin and F. H. M. Faisal, Harmonic generation by superintense light scattering from relativistic electrons, *Phys. Rev. A* **54**, 4383 (1996).
- [12] Y. I. Salamin and F. H. M. Faisal, Generation of Compton harmonics by scattering linearly polarized light of arbitrary intensity from free electrons of arbitrary initial velocity, *J. Phys. A: Math. Gen.* **31**, 1319 (1998).
- [13] Y. Li and S. V. Milton, Intensity and pulse shape effect on the spectra and the angular distribution of nonlinear Thomson scattering, in *Summaries of Papers Presented at the Lasers and Electro-Optics, CLEO '02, Technical Digest* (IEEE, Piscataway, NJ, 2002), Vol. 1, pp. 334–335.
- [14] Q-H. Park, R. W. Boyd, J. E. Sipe and A. L. Gaeta, Theory of relativistic optical harmonic generation, *IEEE J. Sel. Top. Quantum Electron.* **8**, 413 (2002).
- [15] F. He, Y. Y. Lau, D. P. Umstadter, and R. Kowalczyk, Backscattering of an Intense Laser Beam by an Electron, *Phys. Rev. Lett.* **90**, 055002 (2003).
- [16] J. Gao, Thomson Scattering from Ultrashort and Ultraintense Laser Pulses, *Phys. Rev. Lett.* **93**, 243001 (2004).
- [17] G. A. Krafft, Spectral Distributions of Thomson-Scattered Photons from High-Intensity Pulsed Lasers, *Phys. Rev. Lett.* **92**, 204802 (2004).
- [18] M. Boca and A. Oprea, Thomson scattering in the high intensity regime, *Phys. Scr.* **83**, 055404 (2011).
- [19] S. G. Rykovanov, C. G. R. Geddes, C. B. Schroeder, E. Esarey, and W. P. Leemans, Controlling the spectral shape of nonlinear Thomson scattering with proper laser chirping, *Phys. Rev. Accel. Beams* **19**, 030701 (2016).
- [20] K. Ta Phuoc, A. Rousse, M. Pittman, J. P. Rousseau, V. Malka, S. Fritzler, D. Umstadter, and D. Hulin, X-Ray Radiation from Nonlinear Thomson Scattering of an Intense Femtosecond Laser on Relativistic Electrons in a Helium Plasma, *Phys. Rev. Lett.* **91**, 195001 (2003).
- [21] K. Ta Phuoc, F. Burgy, J.-P. Rousseau, and A. Rousse, Nonlinear Thomson scattering from relativistic laser plasma interaction, *Eur. Phys. J. D* **33**, 301 (2005).
- [22] M. Babzien, I. Ben-Zvi, K. Kusche, I. V. Pavlishin, I. V. Pogorelsky, D. P. Siddons, and V. Yakimenko, D. Cline, F. Zhou, T. Hirose, Y. Kamiya, T. Kumita, T. Omori, J. Urakawa, and K. Yokoya, Observation of the Second Harmonic in Thomson Scattering from Relativistic Electrons, *Phys. Rev. Lett.* **96**, 054802 (2006).
- [23] T. Kumita, Y. Kamiya, M. Babzien, I. Ben-Zvi, K. Kusche, I. V. Pavlishin, I. V. Pogorelsky, D. P. Siddons, V. Yakimenko, T. Hirose, T. Omori, J. Urakawa, K. Yokoya, D. Cline, and F. Zhou, Observation of the nonlinear effect in relativistic Thomson scattering of electron and laser beams, *Laser Phys.* **16**, 267 (2006).
- [24] G. Sarri, D. J. Corvan, W. Schumaker, J. M. Cole, A. Di Piazza, H. Ahmed, C. Harvey, C. H. Keitel, K. Krushelnick, S. P. D. Mangles, Z. Najmudin, D. Szymes, A. G. R. Thomas, M. Yeung, Z. Zhao, and M. Zepf, Ultrahigh Brilliance Multi-MeV γ -Ray Beams from Nonlinear Relativistic Thomson Scattering, *Phys. Rev. Lett.* **113**, 224801 (2014).
- [25] K. Khrennikov, J. Wenz, A. Buck, J. Xu, M. Heigoldt, L. Veisz, and S. Karsch, Tunable All-Optical Quasimonochromatic Thomson X-Ray Source in the Nonlinear Regime, *Phys. Rev. Lett.* **114**, 195003 (2015).
- [26] Y. Sakai, I. Pogorelsky, O. Williams, F. O'Shea, S. Barber, I. Gadjev, J. Duris, P. Musumeci, M. Fedurin, A. Korostyshevsky, B. Malone, C. Swinson, G. Stenby, K. Kusche, M. Babzien, M. Montemagno, P. Jacob, Z. Zhong, M. Polyanskiy, V. Yakimenko, and J. Rosenzweig, Observation of redshifting and harmonic radiation in inverse Compton scattering, *Phys. Rev. Spec. Top. Accel. Beams* **18**, 060702 (2015).
- [27] W. Yan, C. Fruhling, G. Golovin, D. Haden, J. Luo, P. Zhang, B. Zhao, J. Zhang, C. Liu, M. Chen, S. Chen, S. Banerjee, and D. Umstadter, High-order multiphoton Thomson scattering, *Nat. Photonics* **11**, 514 (2017).
- [28] T. J. Englert and E. A. Rinehart, Second-harmonic photons from the interaction of free electrons with intense laser radiation, *Phys. Rev. A* **28**, 1539 (1983).
- [29] S.-Y. Chen, A. Maksimchuk, and D. Umstadter, Experimental observation of relativistic nonlinear Thomson Scattering, *Nature* **396**, 653 (1998).
- [30] S.-Y. Chen, A. Maksimchuk, E. Esarey, and D. Umstadter, Observation of Phase-Matched Relativistic Harmonic Generation, *Phys. Rev. Lett.* **84**, 5528 (2000).
- [31] M. Iinuma, K. Matsukado, I. Endo, M. Hashida, K. Hayashi, A. Kohara, F. Matsumoto, Y. Nakanishi, S. Sakabe, S. Shimizu, T. Tauchi, K. Yamamoto, and T. Takahashi, Observation of second harmonics in laser–electron scattering using low energy electron beam, *Phys. Lett. A* **346**, 255 (2005).
- [32] C. Z. He, A. Longman, J. A. Pérez-Hernandez, M. de Marco, C. Salgado, G. Zeraoui, G. Gatti, L. Roso, R. Fedosejevs, and

- W. T. Hill, III, Towards an in situ, full-power gauge of the focal-volume intensity of petawatt-class lasers, *Opt. Express* **27**, 30020 (2019).
- [33] W. L. Erikson and S. Singh, Polarization properties of Maxwell-Gaussian laser beams, *Phys. Rev. E* **49**, 5778 (1994).
- [34] J. Peatross, M. Berrondo, D. Smith, and M. Ware, Vector fields in a tight laser focus: Comparison of models, *Opt. Express* **25**, 13990 (2017).
- [35] J. D. Jackson, *Classical Electrodynamics*, 3rd ed. (Wiley, New York, 1998), Eq. (14.14).
- [36] S. Augst, D. Strickland, D. D. Meyerhofer, S. L. Chin, and J. H. Eberly, Tunneling Ionization of Noble Gases in a High-Intensity Laser Field, *Phys. Rev. Lett.* **63**, 2212 (1989).
- [37] M. Ware, E. Cunningham, C. Coburn, and J. Peatross, Measured photoemission from electron wave packets in a strong laser field, *Opt. Lett.* **41**, 689 (2016).